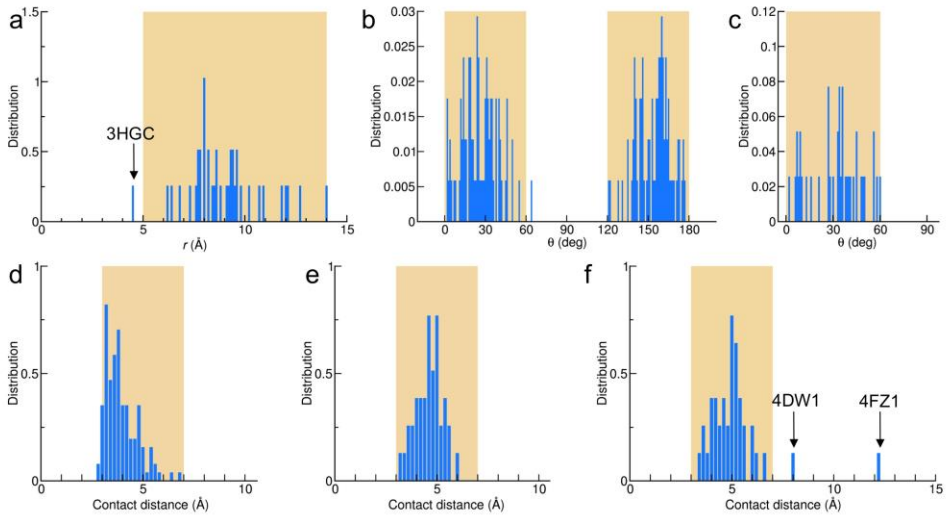

Supplementary Figure 1 | Distributions of distances and angles for transmembrane helices. (**a**) Distribution of the radial distance *r* for the pore-lining helix (PLH) bundle in 39 unique ion channel structures. (**b**) Distribution of the tilt angle *θ* for 171 transmembrane helices in 26 membrane proteins. (**c**) Distribution of *θ* for the PLH bundles of the 39 channel structures. (**d**) Distribution of the contact distances of 128 helix pairs in the 26 membrane proteins. (**e**) Distribution of the contact distances between PLHs and their nearest neighboring helices (not necessarily pore-lining) in the 39 channel structures. (**f**) Distribution of the contact distances between neighboring PLHs in the 39 channel structures.

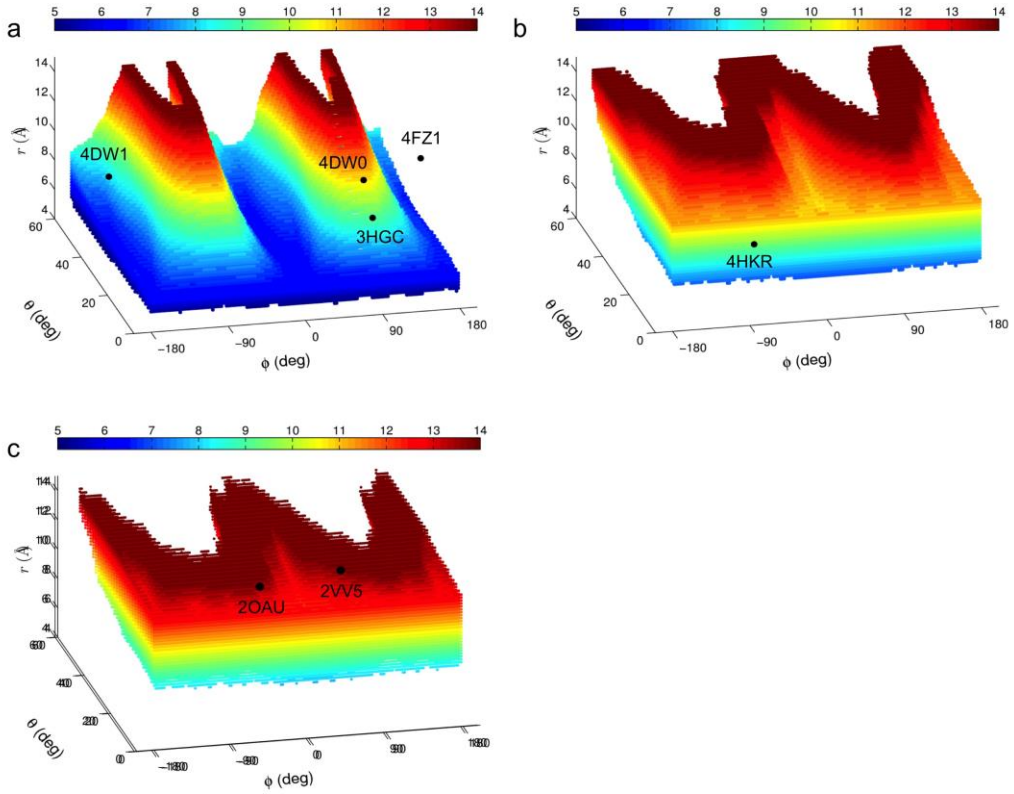

Supplementary Figure 2 | The W-shaped accessible region in the *r*-*θ*-*ϕ* space. (**a**) The accessible region for trimeric models, along with the conformations of 4 actual pore-lining helix (PLH) bundles. The *r* values of the plausible models are displayed according to the color scale at the top. Each black dot represents an actual PLH bundle. The closed-state P2X4 receptor and ASIC1a are within the accessible region, but their open-state counterparts are either near the border of the accessible region (4DW1 for P2X4 receptor) or well outside (4FZ1 for ASIC1a). (**b & c**) Corresponding results for hexamers and heptamers. The hexameric calcium release-activated calcium channel (4HKR) and heptameric MscS (2OAU for closed and 2VV5 for open) are within their respective W-shaped accessible regions.

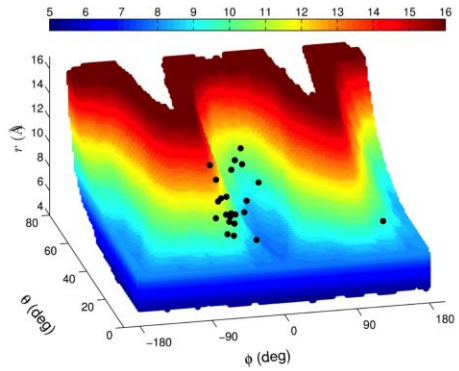

Supplementary Figure 3 | The W-shaped accessible region in the *r*-*θ*-*ϕ* space for tetrameric models. The ranges of parameters are 5 Å < *r* < 16 Å, 0° < *θ* < 80°, and –180° < *ϕ* < 180°. Conformations of pore-lining helix bundles in channel structures are displayed as black dots.

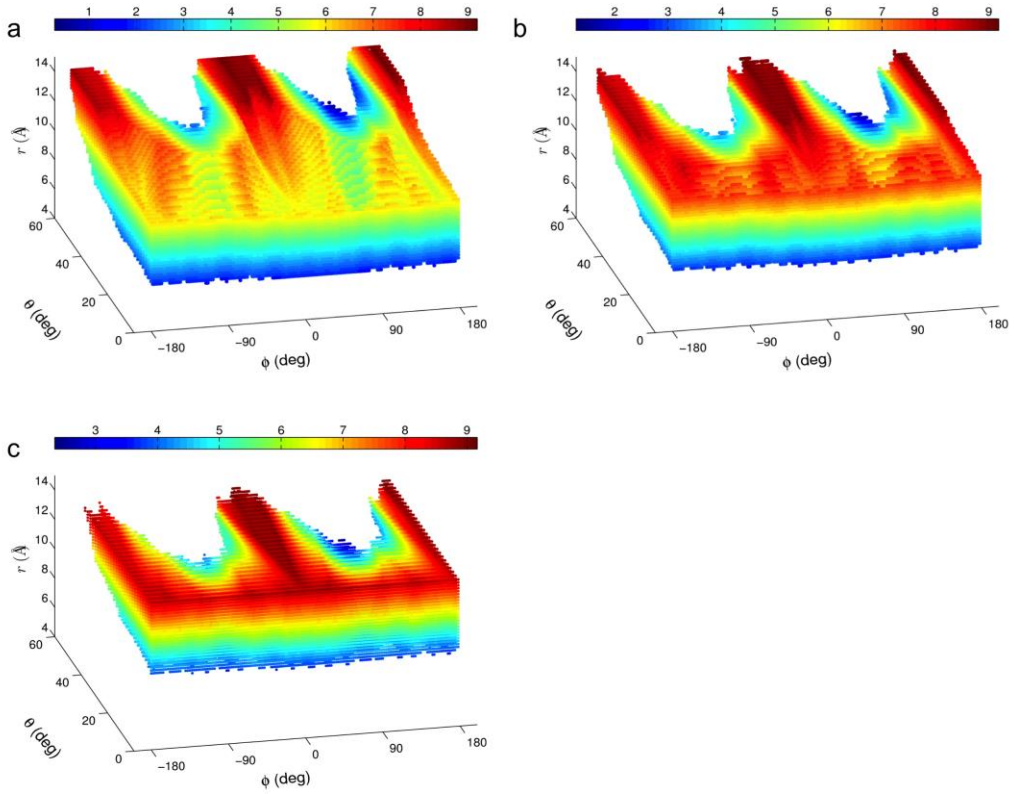

Supplementary Figure 4 | Minimum pore radii of the plausible models. (**a**) Hexamers. (**b**) Heptamers. (**c**) Octamers. In each panel, the R_0 values of the plausible models are displayed according to the color scale at the top.

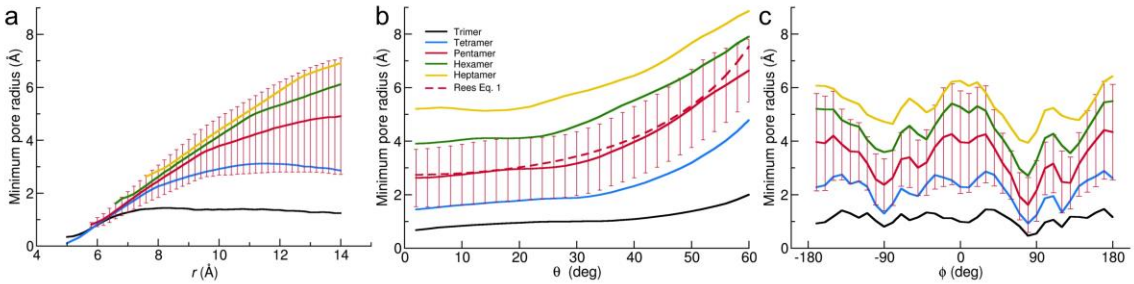

Supplementary Figure 5 | Average R_0 when only one of the three coordinates is fixed, for oligomeric states. (**a**) Averaging at fixed r. (**b**) Averaging at fixed θ. (**c**) Averaging at fixed ϕ. Error bars representing standard deviations are displayed for pentamers, to indicate the significant variations in R_0 when only one coordinate is fixed. In (**b**) the dashed curve displays the prediction of Spencer and Rees for a model of infinite cylinders with a diameter of 7.8 Å.

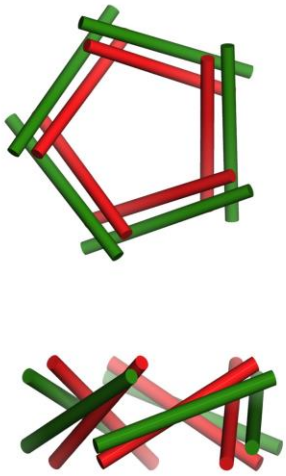

Supplementary Figure 6 | Comparison of the open model proposed in this study for MscL (red) with a model proposed by Sukharev et al. (green). Both top and side views are shown.

Supplementary Table 1 | Oligomeric arrangements of pore-lining helix bundles in channel structures

PDB entry	r (Å)	θ (°)	ϕ (°)	Residues of PLHs	Aligned segment	Ideal helix	rmsd (Å)	Description	Ref.
				Trimers					
3HGC	4.5	44.7	147.0	A-C: V427-E451	427-450	1-24	1.5	ASIC1 desensitized state	[1]
4FZ1	12.7	12.5	153.5	A-C: V427-L450	427-450	1-24	2.0	ASIC1-psalmotoxin 1 at high pH	[2]
4DW0	6.4	49.9	144.5	A-C: I335-I359	335-358	1-24	1.4	P2X4R apo	[3]
4DW1	8.6	45.3	-159.5	A-C: I335-I359	335-358	1-24	1.1	P2X4R with ATP	[3]
				Tetramers					
1BL8	6.8	32.9	-25.1	A-D: L86-Q119	94-117	1-24	0.7	KcsA	[4]
1K4C								KcsA + Fab	[5]
2ITC								KcsA + Fab in NaCl	[6]
2NLJ								KcsA M96V mutant in KCl	[6]
3IGA								KcsA in 150 mM Li^+ and 3 mM K^+	[7]
3HPL								KcsA closed inactivated. E71H and F103A	[8]
3OR7								KcsA E71I	[9]
3OR6								KcsA E71Q	[9]
3STL								KcsA Y82C with cadmium	[10]
3FB8								KcsA open conductive. Open 20 Å	[11]
3EFF								Full length KcsA closed	[12]
3PJS								Full length KcsA open	[13]
3F7Y								KcsA partially open. Open 17 Å	[11]
3FB6	7.8	40.0	-4.0	A-D: L86-F114	94-114	1-21	0.6	KcsA partially open. Open 16 Å	[11]
3FB5								KcsA partially open. Open 14.5 Å	[11]
3F5W	9.8	56.1	11.8	A-D: L86-Q117	94-117	1-24	1.7	KcsA open inactivated. Open 32 Å	[11]
3FB7								KcsA in open state with Rb^+	[8]
3F7V								KcsA open inactivated. Open 23 Å	[11]
2A0L	9.2	57.8	0.4	A-D: P207-K237	214-237	1-24	1.4	KvAP + Fv fragment	[14]
1ORQ								KvAP + Fab	[15]
2A79	7.7	48.4	8.6	A-D: I385-T421	394-417	1-24	1.6	Kv1.2	[16]
3LUT								Full length Kv1.2	[17]
2R9R								Kv1.2/Kv2.1	[18]
3LNM								Kv1.2/Kv2.1 F233W	[19]
4H33	6.2	33.8	4.1	A-D: P68-T102	79-102	1-24	1.1	KvLm closed	[20]
4H37								KvLm in K^+ condition	[20]
3LDC	10.2	55.9	2.6	A-D: P70-I99	76-99	1-24	1.7	MthK K^+ channel	[21]
1LNQ								MthK K^+ channel, Ca^{2+} gated	[22]
4HYO								MthK K^+ channel. S68H & V77C	[23]
4GX5	12.1	28.0	-53.0	A-D: S78-F108	79-99	1-21	1.4	GsuK wild-type	[24]
4GX0								GsuK L97D	[24]
4GX1								GsuK L97D with ADP	[24]
4GX2								GsuK L97D with NAD^+	[24]
3JYC	9.6	35.8	-37.9	A-D:	160-183	1-24	0.6	Kir2.2	[25]

				C155-K183					
3SPI								Kir2.2 with PIP_2	26
3SPC								Kir2.2 with DGPP	26
3SPH								Kir2.2 I223L mutant with PIP_2	26
3SPJ								Kir2.2 I223L mutant apo	26
3SPG								Kir2.2 R186A mutant with PIP_2	26
				A-D:					
2QKS	8.2	34.4	-27.9	V103-S132	109-132	1-24	0.6	Kir3.1	27
				A-D:				GIRK2 (Kir3.2) + PIP_2 + G-	
4KFM	8.8	43.2	-22.6	P167-S196	173-196	1-24	1.1	protein βγ subunits + Na^+	28
3SYO								GIRK2 (Kir3.2)	29
3SYA								GIRK2 (Kir3.2) + PIP_2	29
3SYP								GIRK2 (Kir3.2) R201A mutant	29
3SYQ								GIRK2 (Kir3.2) R201A mutant + PIP_2	29
3SYC								GIRK2 (Kir3.2) D228N mutant	29
				A-D:					
1P7B	8.0	32.7	-31.0	T120-A150	127-150	1-24	0.6	KirBac1.1	30
				A-D:					
2WLJ	7.7	33.7	-23.4	G106-T136	113-136	1-24	0.6	KirBac3.1 semi-latched	31
2WLK								KirBac3.1 latched	31
2WLI								KirBac3.1 semi-latched 3.09 Å	31
2WLO								KirBac3.1 semi-latched 4.20 Å	31
2WLM								KirBac3.1 semi-latched 3.61 Å	31
2WLN								KirBac3.1 unlatched 3.44 Å	31
2WLH								KirBac3.1 unlatched 3.28 Å	31
2X6A								KirBac3.1 Q170A stalled	31
2X6B								KirBac3.1 Q170A blocked with Ba^{2+}	31
2X6C								KirBac3.1 Q170A conductive	31
				A-D:					
3ZRS	7.6	40.6	-14.3	G106-T136	113-136	1-24	0.9	KirBac3.1 open	32
				A-D:					
3BEH	8.0	35.8	-44.1	S185-G213	190-213	1-24	0.6	MlotiK1	33
				A-D:					
2AHY	9.3	27	-41.7	D74-Q103	80-103	1-24	0.4	NaK closed	34
2Q67								NaK channel with Ca^{2+}, D66A	35
3VOU								NaK channel chimera with grafted C-terminal of a NaV channel	36
				A-D:					
3E86	10.7	59.5	13.9	D74-V112	83-103	2-22	1.7	NaK open	37
3K0D								CNG-mimicking NaK channel	38
3OUF								NaK channel K^+ selective mutant	39
3T1C								NaK/NaK2K channel mutant	40
				A-B:Y193-					
3RVY	9.5	34.7	-42.7	M221	198-221	1-24	0.7	NaVAb I217C mutant	41
4DXW								NaVRh	42
3RW0								NaVAb M221C	41
4LTO								NavAe1p	43
4EKW								NaV closed	44
				A-D:					
4F4L	12.0	39.1	-47.7	W71-I93	71-93	2-24	1.0	NaV open	45
				A-D:					
3KG2	7.3	30.2	-36.2	S595-V626	603-626	1-24	0.5	GluA2	46
				A-D:					
2L0J	7.8	26.5	153.1	D24-F47	24-47	1-24	1.2	M2 in hydrated lipid bilayer	47
2RLF								M2 with rimantadine	48
3BKD								M2 crystal structure	49
3C9J								M2 + amantadine crystal structure	49
3LBW								M2 transmembrane domain crystal structure	50

2LY0								M2 S31N mutant with M2WJ332	[51]
2KIX								M2 proton channel influenza B	[52]
2LJB								M2A-M2B chimera	[53]
2LJC								M2A-M2B with rimantadine	[53]
3HZQ	9.1	48.6	23.7	A-D: V14-I46	14-37	1-24	1.0	Tetrameric MscL	[54]
3J5P	8.0	38.3	-22.4	A-D: F655-I689	666-689	1-24	1.9	TRPV1 closed	[55]
3J5Q								TRPV1 with RTX	[56]
3J5R								TRPV1 with capsaicin	[56]
					Pentamers				
2OAR	8.4	36.3	28.2	A-E: N13-I46	13-36	1-24	0.7	MscL	[57]
3RHW	9.4	7.3	68.7	A-E: A241-Q266	241-264	1-24	0.8	GluCl receptor with Fab and ivermectin	[58]
2M6I	11.8	16.3	79.9	A-E: A249-Q266	249-266	1-18	1.0	GlyR receptor transmembrane domain NMR	[59]
1OED	9.6	7.4	67.4	A-E: K242/ 248/256/24 2/251-S269 /L275/L283 /S269/L278	242/248/ 256/242/ 251-265/ 271/279/ 265/274	1-24	0.8	nAChR closed	[60]
2BG9								nAChR refined	[61]
4AQ5								nAChR closed class	[62]
4AQ9								nAChR open class	[62]
2VL0	8.6	9.1	-167.7	A-E: S226-L252	229-252	1-24	0.8	ELIC	[63]
4A97								ELIC with zopiclone	[64]
3UQ7								ELIC L240S F247L in 10 mM cysteamine	[65]
3RQW								ELIC with acetylcholine	[66]
3RQU								ELIC apo	[66]
3ZKR								ELIC with bromoform	[67]
3TLS	8.2	10.3	178.8	A-E: Y221-P243	221-243	1-23	1.1	GLIC E19'P locally closed LC2	[68]
3TLV								GLIC loop2-22' oxidized locally closed LC3	[68]
3TLT								GLIC H11'F locally closed LC1	[68]
3UU3								GLIC loop2-20' oxidized locally closed LC1	[68]
3UU4								GLIC loop2-21' reduced in crystal locally closed LC1	[68]
3TLU								GLIC loop2-24' oxidized locally closed LC1	[68]
3TLW								GLIC loop2-21' oxidized locally closed LC2	[68]
4NPQ								GLIC WT resting state	[69]
3EAM	9.4	5.7	92.5	A-E: S220-T244	220-243	1-24	0.7	GLIC open	[70]
3UU5								GLIC loop2-20' reduced open	[68]
3UUB								GLIC loop2-21' reduced in solution open	[68]
3UU6								GLIC loop2-22' reduced open	[68]
3UU8								GLIC loop2-24' reduced open	[68]
3EHZ								GLIC open	[71]
4HFI								GLIC open	[72]
2XQA								GLIC wildtype TBSb complex	[73]
3P50								GLIC with propofol anesthetic	[74]
4F8H								GLIC with ketamine anesthetic	[75]
4NPP								GLIC WT open	[69]
2KYV	8.0	7.7	179.9	A-E: A24-L52	24-47	1-24	0.6	Phospholamban in T-state	[76]

2M3B								Phosphorylated phospholamban	[77]
2BBJ	8.5	20.9	-168.1	A-E: N285-M302	285-302	7-24	1.0	CorA	[78]
2IUB								CorA	[79]
2HN2								CorA	[80]
4EEB								CorA in the absence of Mg2+	[81]
4EED								CorA in the presence of Mg2+	[81]
4EV6								CorA	[82]
					Hexamer				
4HKR	9.3	1.5	-82.7	A-F: T144-Q180	157-180	1-24	1.0	Calcium release-activated calcium channel (CRAC)	[83]
					Heptamers				
2OAU	10.9	26.9	-12.3	A-G: T93-L111	93-111	6-24	0.9	*E. Coli* MscS	[84]
3T9N								*Thermoanaerobacter Tengcongensis* MscS	[85]
4HW9								*helicobacter pylori* MscS	[86]
2VV5	14.0	9.3	55.0	A-G: T93-L111	93-111	1-19	0.6	*E. Coli* MscS A106V mutant	[87]
2HWA								*E. Coli* open wild type MscS	[86]
4AGE								*E. Coli* open D67C MscS	[88]
4AGF								*E. Coli* open L124C MscS	[88]

Only entries shown in black were deemed “unique”; entries in gray were deemed similar to the preceding entries in black. There are a total of 138 entries, of which 39 are unique.

Supplementary References

1. Gonzales, E.B., Kawate, T. & Gouaux, E. Pore architecture and ion sites in acid-sensing ion channels and P2X receptors. *Nature* **460**, 599-604 (2009).
2. Baconguis, I. & Gouaux, E. Structural plasticity and dynamic selectivity of acid-sensing ion channel-spider toxin complexes. *Nature* **489**, 400-5 (2012).
3. Hattori, M. & Gouaux, E. Molecular mechanism of ATP binding and ion channel activation in P2X receptors. *Nature* **485**, 207-12 (2012).
4. Doyle, D.A. et al. The structure of the potassium channel: molecular basis of K+ conduction and selectivity. *Science* **280**, 69-77 (1998).
5. Zhou, Y., Morais-Cabral, J.H., Kaufman, A. & MacKinnon, R. Chemistry of ion coordination and hydration revealed by a K+ channel-Fab complex at 2.0 A resolution. *Nature* **414**, 43-8 (2001).
6. Lockless, S.W., Zhou, M. & MacKinnon, R. Structural and thermodynamic properties of selective ion binding in a K+ channel. *PLoS Biol* **5**, e121 (2007).
7. Thompson, A.N. et al. Mechanism of potassium-channel selectivity revealed by Na(+) and Li(+) binding sites within the KcsA pore. *Nat Struct Mol Biol* **16**, 1317-24 (2009).
8. Cuello, L.G. et al. Structural basis for the coupling between activation and inactivation gates in K(+) channels. *Nature* **466**, 272-5 (2010).
9. Chakrapani, S. et al. On the structural basis of modal gating behavior in K(+) channels. *Nat Struct Mol Biol* **18**, 67-74 (2011).
10. Raghuraman, H. et al. Mechanism of Cd2+ coordination during slow inactivation in potassium channels. *Structure* **20**, 1332-42 (2012).
11. Cuello, L.G., Jogini, V., Cortes, D.M. & Perozo, E. Structural mechanism of C-type inactivation in K(+) channels. *Nature* **466**, 203-8 (2010).
12. Uysal, S. et al. Crystal structure of full-length KcsA in its closed conformation. *Proc Natl Acad Sci U S A* **106**, 6644-9 (2009).
13. Uysal, S. et al. Mechanism of activation gating in the full-length KcsA K+ channel. *Proc Natl Acad Sci U S A* **108**, 11896-9 (2011).
14. Lee, S.Y., Lee, A., Chen, J. & MacKinnon, R. Structure of the KvAP voltage-

dependent K+ channel and its dependence on the lipid membrane. *Proc Natl Acad Sci U S A* **102**, 15441-6 (2005).

15. Jiang, Y. et al. X-ray structure of a voltage-dependent K+ channel. *Nature* **423**, 33-41 (2003).
16. Long, S.B., Campbell, E.B. & Mackinnon, R. Crystal structure of a mammalian voltage-dependent Shaker family K+ channel. *Science* **309**, 897-903 (2005).
17. Chen, X., Wang, Q., Ni, F. & Ma, J. Structure of the full-length Shaker potassium channel Kv1.2 by normal-mode-based X-ray crystallographic refinement. *Proc Natl Acad Sci U S A* **107**, 11352-7 (2010).
18. Long, S.B., Tao, X., Campbell, E.B. & MacKinnon, R. Atomic structure of a voltage-dependent K+ channel in a lipid membrane-like environment. *Nature* **450**, 376-82 (2007).
19. Tao, X., Lee, A., Limapichat, W., Dougherty, D.A. & MacKinnon, R. A gating charge transfer center in voltage sensors. *Science* **328**, 67-73 (2010).
20. Santos, J.S. et al. Crystal structure of a voltage-gated K+ channel pore module in a closed state in lipid membranes. *J Biol Chem* **287**, 43063-70 (2012).
21. Ye, S., Li, Y. & Jiang, Y. Novel insights into K+ selectivity from high-resolution structures of an open K+ channel pore. *Nat Struct Mol Biol* **17**, 1019-23 (2010).
22. Jiang, Y. et al. Crystal structure and mechanism of a calcium-gated potassium channel. *Nature* **417**, 515-22 (2002).
23. Posson, D.J., McCoy, J.G. & Nimigean, C.M. The voltage-dependent gate in MthK potassium channels is located at the selectivity filter. *Nat Struct Mol Biol* **20**, 159-66 (2013).
24. Kong, C. et al. Distinct gating mechanisms revealed by the structures of a multi-ligand gated K(+) channel. *Elife* **1**, e00184 (2012).
25. Tao, X., Avalos, J.L., Chen, J. & MacKinnon, R. Crystal structure of the eukaryotic strong inward-rectifier K+ channel Kir2.2 at 3.1 A resolution. *Science* **326**, 1668-74 (2009).
26. Hansen, S.B., Tao, X. & MacKinnon, R. Structural basis of PIP2 activation of the classical inward rectifier K+ channel Kir2.2. *Nature* **477**, 495-8 (2011).
27. Nishida, M., Cadene, M., Chait, B.T. & MacKinnon, R. Crystal structure of a

Kir3.1-prokaryotic Kir channel chimera. *EMBO J* **26**, 4005-15 (2007).

28. Whorton, M.R. & MacKinnon, R. X-ray structure of the mammalian GIRK2-betagamma G-protein complex. *Nature* **498**, 190-7 (2013).
29. Whorton, M.R. & MacKinnon, R. Crystal structure of the mammalian GIRK2 K+ channel and gating regulation by G proteins, PIP2, and sodium. *Cell* **147**, 199-208 (2011).
30. Kuo, A. et al. Crystal structure of the potassium channel KirBac1.1 in the closed state. *Science* **300**, 1922-6 (2003).
31. Clarke, O.B. et al. Domain reorientation and rotation of an intracellular assembly regulate conduction in Kir potassium channels. *Cell* **141**, 1018-29 (2010).
32. Bavro, V.N. et al. Structure of a KirBac potassium channel with an open bundle crossing indicates a mechanism of channel gating. *Nat Struct Mol Biol* **19**, 158-63 (2012).
33. Clayton, G.M., Altieri, S., Heginbotham, L., Unger, V.M. & Morais-Cabral, J.H. Structure of the transmembrane regions of a bacterial cyclic nucleotide-regulated channel. *Proc Natl Acad Sci U S A* **105**, 1511-5 (2008).
34. Shi, N., Ye, S., Alam, A., Chen, L. & Jiang, Y. Atomic structure of a Na+- and K+-conducting channel. *Nature* **440**, 570-4 (2006).
35. Alam, A., Shi, N. & Jiang, Y. Structural insight into Ca2+ specificity in tetrameric cation channels. *Proc Natl Acad Sci U S A* **104**, 15334-9 (2007).
36. Irie, K., Shimomura, T. & Fujiyoshi, Y. The C-terminal helical bundle of the tetrameric prokaryotic sodium channel accelerates the inactivation rate. *Nat Commun* **3**, 793 (2012).
37. Alam, A. & Jiang, Y. High-resolution structure of the open NaK channel. *Nat Struct Mol Biol* **16**, 30-4 (2009).
38. Derebe, M.G., Zeng, W., Li, Y., Alam, A. & Jiang, Y. Structural studies of ion permeation and Ca2+ blockage of a bacterial channel mimicking the cyclic nucleotide-gated channel pore. *Proc Natl Acad Sci U S A* **108**, 592-7 (2011).
39. Derebe, M.G. et al. Tuning the ion selectivity of tetrameric cation channels by changing the number of ion binding sites. *Proc Natl Acad Sci U S A* **108**, 598-602 (2011).

40. Sauer, D.B., Zeng, W., Raghunathan, S. & Jiang, Y. Protein interactions central to stabilizing the K+ channel selectivity filter in a four-sited configuration for selective K+ permeation. *Proc Natl Acad Sci U S A* **108**, 16634-9 (2011).
41. Payandeh, J., Scheuer, T., Zheng, N. & Catterall, W.A. The crystal structure of a voltage-gated sodium channel. *Nature* **475**, 353-8 (2011).
42. Zhang, X. et al. Crystal structure of an orthologue of the NaChBac voltage-gated sodium channel. *Nature* **486**, 130-4 (2012).
43. Shaya, D. et al. Structure of a prokaryotic sodium channel pore reveals essential gating elements and an outer ion binding site common to eukaryotic channels. *J Mol Biol* **426**, 467-83 (2014).
44. Payandeh, J., Gamal El-Din, T.M., Scheuer, T., Zheng, N. & Catterall, W.A. Crystal structure of a voltage-gated sodium channel in two potentially inactivated states. *Nature* **486**, 135-9 (2012).
45. McCusker, E.C. et al. Structure of a bacterial voltage-gated sodium channel pore reveals mechanisms of opening and closing. *Nat Commun* **3**, 1102 (2012).
46. Sobolevsky, A.I., Rosconi, M.P. & Gouaux, E. X-ray structure, symmetry and mechanism of an AMPA-subtype glutamate receptor. *Nature* **462**, 745-56 (2009).
47. Sharma, M. et al. Insight into the mechanism of the influenza A proton channel from a structure in a lipid bilayer. *Science* **330**, 509-12 (2010).
48. Schnell, J.R. & Chou, J.J. Structure and mechanism of the M2 proton channel of influenza A virus. *Nature* **451**, 591-5 (2008).
49. Stouffer, A.L. et al. Structural basis for the function and inhibition of an influenza virus proton channel. *Nature* **451**, 596-9 (2008).
50. Acharya, R. et al. Structure and mechanism of proton transport through the transmembrane tetrameric M2 protein bundle of the influenza A virus. *Proc Natl Acad Sci U S A* **107**, 15075-80 (2010).
51. Wang, J. et al. Structure and inhibition of the drug-resistant S31N mutant of the M2 ion channel of influenza A virus. *Proc Natl Acad Sci U S A* **110**, 1315-20 (2013).
52. Wang, J., Pielak, R.M., McClintock, M.A. & Chou, J.J. Solution structure and functional analysis of the influenza B proton channel. *Nat Struct Mol Biol* **16**,

1267-71 (2009).

53. Pielak, R.M., Oxenoid, K. & Chou, J.J. Structural investigation of rimantadine inhibition of the AM2-BM2 chimera channel of influenza viruses. *Structure* **19**, 1655-63 (2011).

54. Liu, Z., Gandhi, C.S. & Rees, D.C. Structure of a tetrameric MscL in an expanded intermediate state. *Nature* **461**, 120-4 (2009).

55. Liao, M., Cao, E., Julius, D. & Cheng, Y. Structure of the TRPV1 ion channel determined by electron cryo-microscopy. *Nature* **504**, 107-12 (2013).

56. Cao, E., Liao, M., Cheng, Y. & Julius, D. TRPV1 structures in distinct conformations reveal activation mechanisms. *Nature* **504**, 113-8 (2013).

57. Chang, G., Spencer, R.H., Lee, A.T., Barclay, M.T. & Rees, D.C. Structure of the MscL homolog from Mycobacterium tuberculosis: a gated mechanosensitive ion channel. *Science* **282**, 2220-6 (1998).

58. Hibbs, R.E. & Gouaux, E. Principles of activation and permeation in an anion-selective Cys-loop receptor. *Nature* **474**, 54-60 (2011).

59. Mowrey, D.D. et al. Open-channel structures of the human glycine receptor alpha1 full-length transmembrane domain. *Structure* **21**, 1897-904 (2013).

60. Miyazawa, A., Fujiyoshi, Y. & Unwin, N. Structure and gating mechanism of the acetylcholine receptor pore. *Nature* **423**, 949-55 (2003).

61. Unwin, N. Refined structure of the nicotinic acetylcholine receptor at 4A resolution. *J Mol Biol* **346**, 967-89 (2005).

62. Unwin, N. & Fujiyoshi, Y. Gating movement of acetylcholine receptor caught by plunge-freezing. *J Mol Biol* **422**, 617-34 (2012).

63. Hilf, R.J. & Dutzler, R. X-ray structure of a prokaryotic pentameric ligand-gated ion channel. *Nature* **452**, 375-9 (2008).

64. Spurny, R. et al. Pentameric ligand-gated ion channel ELIC is activated by GABA and modulated by benzodiazepines. *Proc Natl Acad Sci U S A* **109**, E3028-34 (2012).

65. Gonzalez-Gutierrez, G. et al. Mutations that stabilize the open state of the Erwinia chrisanthemi ligand-gated ion channel fail to change the conformation of the pore domain in crystals. *Proc Natl Acad Sci U S A* **109**, 6331-6 (2012).

66. Pan, J. et al. Structure of the pentameric ligand-gated ion channel ELIC cocrystallized with its competitive antagonist acetylcholine. *Nat Commun* **3**, 714 (2012).
67. Spurny, R. et al. Multisite binding of a general anesthetic to the prokaryotic pentameric Erwinia chrysanthemi ligand-gated ion channel (ELIC). *J Biol Chem* **288**, 8355-64 (2013).
68. Prevost, M.S. et al. A locally closed conformation of a bacterial pentameric proton-gated ion channel. *Nat Struct Mol Biol* **19**, 642-9 (2012).
69. Sauguet, L. et al. Crystal structures of a pentameric ligand-gated ion channel provide a mechanism for activation. *Proc Natl Acad Sci U S A* **111**, 966-71 (2014).
70. Bocquet, N. et al. X-ray structure of a pentameric ligand-gated ion channel in an apparently open conformation. *Nature* **457**, 111-4 (2009).
71. Hilf, R.J. & Dutzler, R. Structure of a potentially open state of a proton-activated pentameric ligand-gated ion channel. *Nature* **457**, 115-8 (2009).
72. Sauguet, L. et al. Structural basis for ion permeation mechanism in pentameric ligand-gated ion channels. *EMBO J* **32**, 728-41 (2013).
73. Hilf, R.J. et al. Structural basis of open channel block in a prokaryotic pentameric ligand-gated ion channel. *Nat Struct Mol Biol* **17**, 1330-6 (2010).
74. Nury, H. et al. X-ray structures of general anaesthetics bound to a pentameric ligand-gated ion channel. *Nature* **469**, 428-31 (2011).
75. Pan, J. et al. Structure of the pentameric ligand-gated ion channel GLIC bound with anesthetic ketamine. *Structure* **20**, 1463-9 (2012).
76. Verardi, R., Shi, L., Traaseth, N.J., Walsh, N. & Veglia, G. Structural topology of phospholamban pentamer in lipid bilayers by a hybrid solution and solid-state NMR method. *Proc Natl Acad Sci U S A* **108**, 9101-6 (2011).
77. Vostrikov, V.V., Mote, K.R., Verardi, R. & Veglia, G. Structural dynamics and topology of phosphorylated phospholamban homopentamer reveal its role in the regulation of calcium transport. *Structure* **21**, 2119-30 (2013).
78. Lunin, V.V. et al. Crystal structure of the CorA Mg2+ transporter. *Nature* **440**, 833-7 (2006).

79. Eshaghi, S. et al. Crystal structure of a divalent metal ion transporter CorA at 2.9 angstrom resolution. *Science* **313**, 354-7 (2006).
80. Payandeh, J. & Pai, E.F. A structural basis for Mg2+ homeostasis and the CorA translocation cycle. *EMBO J* **25**, 3762-73 (2006).
81. Pfoh, R. et al. Structural asymmetry in the magnesium channel CorA points to sequential allosteric regulation. *Proc Natl Acad Sci U S A* **109**, 18809-14 (2012).
82. Guskov, A. et al. Structural insights into the mechanisms of Mg2+ uptake, transport, and gating by CorA. *Proc Natl Acad Sci U S A* **109**, 18459-64 (2012).
83. Hou, X., Pedi, L., Diver, M.M. & Long, S.B. Crystal structure of the calcium release-activated calcium channel Orai. *Science* **338**, 1308-13 (2012).
84. Bass, R.B., Strop, P., Barclay, M. & Rees, D.C. Crystal structure of Escherichia coli MscS, a voltage-modulated and mechanosensitive channel. *Science* **298**, 1582-7 (2002).
85. Zhang, X. et al. Structure and molecular mechanism of an anion-selective mechanosensitive channel of small conductance. *Proc Natl Acad Sci U S A* **109**, 18180-5 (2012).
86. Lai, J.Y., Poon, Y.S., Kaiser, J.T. & Rees, D.C. Open and shut: crystal structures of the dodecylmaltoside solubilized mechanosensitive channel of small conductance from Escherichia coli and Helicobacter pylori at 4.4 A and 4.1 A resolutions. *Protein Sci* **22**, 502-9 (2013).
87. Wang, W. et al. The structure of an open form of an E. coli mechanosensitive channel at 3.45 A resolution. *Science* **321**, 1179-83 (2008).
88. Pliotas, C. et al. Conformational state of the MscS mechanosensitive channel in solution revealed by pulsed electron-electron double resonance (PELDOR) spectroscopy. *Proc Natl Acad Sci U S A* **109**, E2675-82 (2012).